Bioinformatics Domain Structure Prediction and Homology Modeling of Human Ryanodine Receptor 2

Bauerová-Hlinková V.[1] et al.*
*Institute of Molecular Biology, Slovak Academy of Sciences, Bratislava,
Slovakia*

1. Introduction

Ryanodine receptors (RyRs) are homotetrameric intracellular calcium release channels in the membranes of the endoplasmic (ER) and sarcoplasmic reticulum (SR) (George et al. 2005, Meissner 2002, 2004). Each subunit consists of ~5000 amino acid residues (George et al. 2005). There are three isoforms of the ryanodine receptor: the RyR1 isoform is expressed predominantly in skeletal muscle, the RyR2 isoform predominates in cardiac muscle, and the RyR3 isoform is expressed in a variety of tissues (Sorrentino 1995). In the mammalian heart, the RyR2 isoform is a principal component of the excitation-contraction (E-C) coupling process. Action potential depolarization of the cardiac cell results in injection of calcium ions into the cell via calcium channels (dihydropyridine receptors, DHPRs). This small calcium influx then drives the release of calcium from intracellular calcium stores by triggering the opening of RyR2 channels (Fabiato 1985). The released calcium causes contraction by binding to troponin C (Ebashi and Ogawa 1988). Consequently, precise regulation of RyR activity during heartbeat is essential to proper cardiac function.

In several cardiac diseases, such as heart failure and the genetic diseases CVPT (catecholaminergic polymorphic ventricular tachycardia) and ARVD2 (arrhythmogenic right ventricular dysplasia), the function of RyR is compromised. In heart failure, the release of calcium in response to the action potential is decreased, while RyR remains more active during the diastole (Durham et al. 2007, Yano et al. 2006). In CPVT and ARVD2, RyRs contain mutations that lead to altered RyR activity which may result in premature calcium release in the absence of an action potential (Durham et al. 2007, Yano et al. 2006).

In this work we present a bioinformatics analysis of the whole of human RyR2 (hRyR2) in context with the available functional information, in order to locate individual domains for further biochemical and structural studies. The reliability of the predictions in the N-terminal region (Bauerova-Hlinkova et al. 2010) was verified experimentally by expressing and characterizing the domains identified. We also describe the results of a CD-

---
* Bauer J.[1], Hostinová E.[1], Gašperík J.[1], Beck K.[3], Borko Ľ.[1], Faltínová A.[2], Zahradníková A.[2] and Ševčík J.[1]
[2]*Institute of Molecular Physiology and Genetics, Slovak Academy of Sciences, Bratislava, Slovakia*
[3]*School of Dentistry, Cardiff University, Heath Park, Cardiff, Wales, UK*

spectroscopy study we carried out in order to determine the domain organization of RyR2; this study also included an analysis of the secondary structure elements of the N-terminal part of RyR2. Finally, we present a homology model of the N-terminal part of RyR2 which is based on the recently determined X-ray structure of rabbit RyR1. The amino-acid sequence identity of these two proteins is more than 80%, which suggests that predictions made from this model will most likely be reliable. The homology model agrees with our bioinformatics analysis and also with the results of our CD-spectroscopy study. This model should help to locate and identify the mutations and the residues in their proximity that are responsible for the cardiac diseases CPVT1 and ARVD2.

2. Physiological function of RyR2

Calcium release from intracellular stores is mediated by two types of calcium release channels ─ ryanodine receptors (RyRs) and inositol trisphosphate receptors (IP3Rs) (Berridge 1994). These channels are expressed in most tissues. RyRs play a primary role in skeletal and cardiac muscle cells, where they mediate muscle contraction. In these tissues IP3Rs play only a modulatory role. In contrast, smooth muscle, neurons and non-excitable tissues rely on IP3R to play the primary role in calcium release, while RyRs play a modulatory role (Berridge 1994). The study of RyRs is therefore mostly concerned with understanding their role in the activation of skeletal and cardiac muscle contraction.

2.1 Ion permeation

The physiological role of the RyR is to allow permeation of Ca^{2+} ions from the lumen of the SR into the cytosol. Although the calcium gradient between these two compartments is high (the diastolic free Ca^{2+} concentration is only ~100 nM in the cytosol but ~1–2 mM in the SR lumen (Shannon et al. 2003)), concentrations of other ions are much larger (~150 mM K^+) or comparable (~1 mM Mg^{2+}) on both sides of the SR membrane. During the systole, >70% of the Ca^{2+} ions are released from the SR in several milliseconds. Therefore the conductance, which determines the rate of transport, and the permeability of the channel for Ca^{2+} ions, which enables selective transport of Ca^{2+} in the presence of high concentrations of other ions, have to be sufficiently high.

The properties of RyRs have been investigated in planar bilayers by fusion of SR vesicles (Meissner and Henderson (1987), reviewed by Meissner (2002)) and by incorporation of purified ryanodine receptors (Lai et al. (1988), reviewed by Meissner (2002, 2004)) into bilayer membranes. RyRs are characterised by their high conductance and relatively low ion selectivity. Their monovalent cation conductance is very high (200–700 pS), highest for the RyR2 isoform and lowest for the RyR1 isoform, and they are half-saturated at ~10–50 mM concentrations for all monovalent cations. Despite their differences in conductance, their permeability to all monovalents is approximately equal. The channel is 6.5-fold more permeable for divalent than for monovalent ions, and their conductance (90–200 pS) (Williams 1992) increases with the size of the divalent ion. Half-saturation is achieved at ~0.5 mM divalent ion concentration, i.e., at much lower concentrations than for monovalent ions. These properties of the RyR channel enable effective transport of Ca^{2+} ions. The large conductance ensures a sufficient transport rate, while the high calcium affinity ensures that under normal conditions, the rate of Ca^{2+} transport will be close to maximal. The unitary Ca^{2+} current under physiological conditions has been estimated to be

0.4–0.6 pA (Mejia-Alvarez et al. 1999, Kettlun et al. 2003). The permeation properties are conferred on the RyR by the amino acids forming the pore, which are close to the C-terminal end of the RyR (Du et al. 2001, Zhao et al. 1999), and where aa. GGIG were proposed to form the selectivity filter (Balshaw et al. 1999, Gao et al. 2000).

2.2 Regulation by Ca^{2+}

Ca^{2+} ions are the most important regulator of RyR activity (Fabiato 1985). They act at several Ca^{2+} binding sites, leading to activation as well as inactivation of RyR. From the physiological point of view it is important to note that Mg^{2+} ions, present at millimolar concentrations in the cytosol and the SR lumen, are also capable of binding to all RyR Ca^{2+} binding sites. The existence of two activation sites and two inactivation sites has been proposed (Laver 2007, Laver 2009).

2.2.1 Cytosolic activation

Cytosolic Ca^{2+} is the physiological activator of the RyR2 and RyR3 isoforms and contributes to the activation of the RyR1 isoform. In the cardiac myocyte, diastolic Ca^{2+} is ~ 50–100 nM (Baartscheer et al. 1998, Kagaya et al. 1995). Ca^{2+} ions activate RyR channels in the concentration range relevant for excitation-contraction coupling (0.3–100 μM). The probability that RyR channels are open in the absence of other modulators increases with increasing calcium concentration with half-activation at ~1 μM (Chu et al. 1993, Coronado et al. 1994, Gyorke et al. 1994, Meissner 2004, Zahradnikova et al. 1999).
The time course of both RyR activation (Gyorke and Fill 1993, Schiefer et al. 1995, Zahradnikova and Zahradnik 1999, Zahradnikova et al. 1999, Zahradnikova et al. 2003) and deactivation (Schiefer et al. 1995, Velez et al. 1997) is very rapid; the activation rate is dependent on Ca^{2+} concentration (Schiefer et al. 1995, Zahradnikova et al. 1999) while the deactivation rate is not (Schiefer et al. 1995). The fast activation and deactivation kinetics should allow RyRs to respond to physiological calcium signals that last only a few milliseconds. The response of the ryanodine receptor to rapid and brief calcium elevations, mimicking physiological stimuli, has shown that RyR has several Ca^{2+} binding sites. In wild-type RyRs, binding of at least 4 Ca^{2+} ions precedes channel activation (Zahradnikova et al. 1999). RyR channels containing subunits mutated in the putative Ca^{2+} binding sites are less sensitive to activation by cytosolic Ca^{2+} (Li and Chen 2001). Analysis of the calcium dependence of RyR tetramers containing both wild-type and mutated monomers confirmed the presence of a single Ca^{2+} binding site on each of the monomers and revealed that activation by Ca^{2+} proceeds by allosteric interaction between Ca^{2+} binding and channel opening (Zahradnik et al. 2005). The cytosolic Ca^{2+} binding activation site is located in the C-terminal part of the channel (Chen et al. 1998, Li and Chen 2001). The C-terminal part of the RyR sequence (amino acids 3661–5037) is capable of forming an ion channel that can be activated by calcium (Bhat et al. 1997, Xu et al. 2000).
Due to competition between Ca^{2+} and Mg^{2+} ions, the apparent sensitivity of RyR2 channels *in situ* to activation by calcium is decreased about 10 times by Mg^{2+} binding to the activation site (Meissner 1994). The calcium dependence of *in situ* RyR activity enabled elucidation of the mechanism of the differences between the effect of Mg^{2+} and Ca^{2+} on RyR. While binding of Ca^{2+} to the activation site has a strong positively allosteric effect, the binding of Mg^{2+} has a weak negatively allosteric effect (Zahradnikova et al. 2010). At diastolic calcium concentrations, more than 75% of the cytosolic activation sites are occupied by Mg^{2+}

(Zahradnikova et al. 2010). Since Mg^{2+} dissociation from this site is relatively slow (Zahradnikova et al. 2003, 2010), it limits the rate at which RyRs can respond to physiological Ca^{2+} elevations, which might play an important role in the physiological regulation of RyRs.

2.2.2 Luminal activation

Calcium ions also affect RyR activity from the side of the SR lumen. At low cytosolic Ca^{2+} concentrations, when RyR activity is low, the presence of Ca^{2+} at the luminal side increases RyR activity by prolonging channel opening if calcium current flows from the lumen to the cytosol, i.e., by binding to the cytosolic calcium binding site (Laver 2007, Laver 2009, Xu and Meissner 1998). Luminal Ca^{2+} also affects RyR activity by binding to a luminal binding site which may be located either on the channel or on an associated protein (Gaburjakova and Gaburjakova 2006, Gyorke and Gyorke 1998, Gyorke et al. 2004, Qin et al. 2008). The action of luminal Ca^{2+} is complicated by the fact that the SR lumen contains a large amount of calsequestrin, a low-affinity Ca^{2+} buffer, which, in addition to its buffering effect, also interacts with RyR and modulates its activity (see below). In planar lipid bilayers, the effect of luminal Ca^{2+} on RyR activity can be explained by a combination of direct binding to the luminal activation site and of action at the cytosolic sites via "feed-through" of Ca^{2+} that passes through the channel pore to the cytosolic side of the channel (Laver 2007, 2009). Mg^{2+} inhibits the luminal effect of Ca^{2+} by competing with it at the luminal activation site (Laver and Honen 2008).

2.2.3 Inactivation

Their low sensitivity to Ca^{2+}-induced inactivation distinguishes RyR2 and RyR3 from the skeletal isoform, which is half-inactivated by ~100 μM Ca^{2+} (Chu et al. 1993, Lamb 1993, Smith et al. 1988). The identity of the inactivating calcium binding site is unknown. Because of the differences between RyR1 on one hand and RyR2/RyR3 on the other, it is assumed that the differences in sensitivity to calcium-dependent inactivation may be partially due to the divergent region DR1, which differs between these RyR isoforms (Du et al. 2000). The inhibitory site has low specificity—the affinity of Mg^{2+} and Ca^{2+} to this binding site is similar (Gyorke and Gyorke 1998, Laver and Honen 2008, Laver et al. 1997, Xu et al. 1996).

2.2.4 Activation by ATP

ATP increases the probability that the RyR channel will be open (EC_{50} = ~100 μM) without markedly affecting its calcium dependence (Xu et al. 1996). The activity of the RyR1 isoform is potentiated more strongly than that of RyR2 (Zimanyi and Pessah 1991). Although most ATP in the cell is present in the form of $Mg \cdot ATP$, it seems that the activating species is free ATP^{2-} (Copello et al. 2002). Other nucleosides are much less effective than ATP. ADP is a partial agonist with a lower affinity (EC_{50} = ~1 mM). Adenosine and adenine have a still lower effect. CTP, GTP, ITP and UTP do not activate the channel at all (Meissner 2002). The existence of the adenine ring is necessary for ATP binding, and the large effectiveness of channel activation by ATP appears to be caused by the presence of the negatively charged phosphate groups (Chan et al. 2000, 2003).

2.2.5 Modulation by associated proteins

Calmodulin (CaM) is a small Ca^{2+}-binding protein that affects many enzymes, receptors and channels. CaM with four bound calcium ions and apo-CaM without bound Ca^{2+} ions have

different conformations and therefore also different effects. CaM inhibits all RyR isoforms. Apo-CaM has a stimulatory effect on the activity of RyR1 and RyR3, but, depending on conditions, it either does not affect or inhibits the RyR2 isoform. The effects of CaM are mediated by its high-affinity binding to a binding site (amino acids 3583–3603 in RyR2) on each of the monomers, which is conserved in all RyR isoforms. The different CaM effects on the different isoforms are apparently due to differences in the isoforms in a region outside the CaM binding site (Meissner 2004). The locations of bound CaM and apo-CaM on the binding site are different (Meissner 2004), and a calcium-dependent physical relocation of CaM on the RyR molecule has also been observed by cryoelectron microscopy (cryo-EM) (Samso and Wagenknecht 2002). Modulation of RyR activity by calmodulin may therefore involve conformational changes in more distant parts of the RyR protein.

FKBP (FK506-binding protein) belongs to the immunophilins, cytosolic receptors for imunosuppresants such as rapamycin and FK506. Each RyR monomer contains a binding site for either FKBP12 (in RyR1) or FKBP12.6 (in RyR2). The interaction of FKBP with the channel stabilizes the protein complex and supports coordinated gating of all four subunits. It is thought that FKBP also plays a role in coupled gating of neighbouring RyR channels (Williams et al. 2001).

In addition to RyR channels, the SR membrane of terminal cisternae also contains the proteins triadin and junctin (Bers 2004) which associate with RyRs from the luminal side. In the lumen of the terminal cisterna there is also a large quantity of the protein calsequestrin (CSQ), a low-affinity calcium-binding protein that serves as a calcium buffer and also modulates RyR activity in a calcium-dependent manner (Bers 2004). CSQ most probably interacts with the RyR channel through interactions with triadin and junctin, so that for correct luminal regulation all three accessory proteins are necessary (Gyorke et al. 2004, Terentyev et al. 2008).

2.2.6 Modulation by phosphorylation

Ryanodine receptors have several conserved regions that are putative phosphorylation sites. Furthermore, kinases (PKA) and phosphatases (PP1 and PP2A) are directly attached to the channel, suggesting that regulation by phosphorylation may have physiological significance (Marx et al. 2001). The first phosphorylation site discovered on the RyR2 molecule (Witcher et al. 1991) was S2809 (S2843 in RyR1), which can be phosphorylated by the Ca^{2+}/calmodulin-dependent protein kinase II (CaMKII) and to some extent also by PKA. Other kinases, such as PKG and PKC, affect RyRs as well (Takasago et al. 1991), e.g. by changing their ability to bind the alkaloid ryanodine. The mechanisms by which phosphorylation and dephosphorylation induce changes in RyR activity are not clearly understood, however. An increase in RyR activity due to an increase in calcium sensitivity (Marx and Marks 2002), as well as an increase in the rate of adaptation after a rapid calcium increase (Valdivia et al. 1995) have both been observed after phosphorylation.

2.2.7 Interdomain interactions

Most of the mutations that affect RyR2 function in CPVT and ARVD2 are located in either of four domains: the N-terminal domain, the central domain, the cytoplasmic I-domain, and the transmembrane domain. This clustering, as well as the similarity between the effects of mutations at different positions within these domains (hyperactivation of the channel and

increased sensitivity to agonists) led to the postulation of the interdomain hypothesis (Yamamoto et al. 2000). It was hypothesized that there is an interaction between the N-terminal and the central domain that stabilizes the channel in the closed state. Mutations within these domains would then weaken this interdomain interaction (Ikemoto and Yamamoto 2000, Yamamoto et al. 2000) and these changes might play a key role in the regulatory mechanisms of the channel. The experimental strategy to test this hypothesis was based on the assumption that if an interaction between two regions functions as a regulatory mechanism, then a synthetic domain peptide with a sequence identical to that of one of the interacting regions should destabilize the interaction and disturb RyR regulation in a way similar to that observed in the mutations. Several domain peptides from the N-terminal and central region of RyR1 or RyR2 (H163–S195, L590–C609 and L601–C620, L2442–P2477 and G2460–P2495, D2380–A2411) were indeed able to activate RyR and increase its sensitivity to agonists (El-Hayek et al. 1999, Faltinova et al. 2011, Tateishi et al. 2009, Yamamoto and Ikemoto 2002, Yang et al. 2006). The group of Yamamoto and Ikemoto further postulated, based results of George et al. (2004), that the interaction between the I-domain and another, undefined domain also plays a role in stabilizing the closed state of RyR2. A domain peptide from the I-domain (P4090–E4123) did indeed activate RyR2 (Tateishi et al. 2009). Furthermore, mutations in the N-terminal and central domains destabilized the interaction of RyR2 with its regulator calmodulin (Ono et al. 2010). Two RyR-stabilizing drugs that act on the central (K201) and N-terminal domains (dantrolene) antagonized the effect of the central and N-terminal mutations, respectively, and restored calmodulin binding (Ono et al. 2010, Xu et al. 2010). Transmission between the interdomain interaction, calmodulin binding, and channel opening is believed to be mediated by a calmodulin-like domain (residues 4064–4210 in RyR1; (Xiong et al. 2006)) and its interaction with the calmodulin binding domain of RyR (Ono et al. 2010). The effect of CPVT and ARVD2 mutations on the extent of interdomain interaction may be manifested as a change in the intrinsic opening tendency of the channel or in the allosteric effect between calcium binding and channel opening (Zahradnikova et al. 2010).

2.3 Excitation-contraction coupling

The RyRs are located at tubulo-reticular junctions, special calcium release sites, where they face the adjacent calcium channels (DHPRs) of the plasma membrane. The release sites in both skeletal and cardiac muscle contain clusters of RyRs and DHPRs, and their structures are quite similar. However, DHPRs and RyRs are positioned very precisely adjacent to one another in skeletal muscle but not in cardiac muscle (Protasi 2002). Therefore, in contrast to skeletal muscle, where RyR1 is activated by conformational changes in the DHPR protein (Rios and Brum 1987, Rios et al. 1993), in cardiac cells RyRs are activated by calcium ions that flow into the dyadic space during single-channel openings of DHPRs (Fabiato 1985).

Calcium sparks, calcium release events of individual calcium release units (Cheng et al. 1993), raise local cytosolic Ca^{2+} concentrations by ~200 nM (Cannell et al. 1994, Cannell et al. 1995, Cheng et al. 1993, Lopez-Lopez et al. 1995). They can be discerned when release probability is low (Cheng et al. 1993). Although the probability of spontaneous sparks in a rat ventricular myocyte is low (about 100 s^{-1}) (Cheng et al. 1993), openings of L-type Ca^{2+} channels greatly increase this probability during a voltage step depolarization (Cannell et al. 1995, Lopez-Lopez et al. 1995). Ca^{2+} sparks are stereotypical, i.e., their amplitudes and

spatio-temporal properties appear to be independent of their trigger signal (Cannell et al. 1995, Lopez-Lopez et al. 1995). This indicates that the amplitude and time course of a Ca^{2+} spark is largely governed by the properties of the participating RyRs. Thus, Ca^{2+} sparks can be considered to be the elementary Ca^{2+} release events underlying E-C coupling, and gradation of calcium release in response to I_{Ca} can be explained by the summation of variable numbers of Ca^{2+} sparks being activated (Cheng et al. 1996).

Under normal conditions, Ca^{2+} sparks are unable to activate additional Ca^{2+} sparks in adjacent regions, although the local free Ca^{2+} concentration associated with a Ca^{2+} spark is much larger than the global increase in free Ca^{2+} concentration produced by Ca^{2+} current activation ((Cannell et al. 1995), but see Parker et al. (1996)). This observation can be explained by the fact that SR Ca^{2+} release channels are situated very close to the L-type Ca^{2+} channel (the "local control model"; (Stern 1992)), where they sense the > 100-fold increase in local free Ca^{2+} concentration upon opening of a nearby L-type Ca^{2+} channel. The sensitivity of this local control is most clearly seen in the evidence that a single DHPR channel opening can elicit a Ca^{2+} spark (Cannell et al. 1995, Lopez-Lopez et al. 1995, Santana et al. 1996). A detailed analysis revealed that the probability of Ca^{2+} activation depends on the square of the single sarcolemmal Ca^{2+} channel current and on the square of the local free Ca^{2+} concentration (Santana et al. 1996) and that it is quite sensitive to the duration of the DPHR openings (Zahradnikova et al. 1999). Theoretical calculations (Cannell and Soeller 1997) as well as experimental data (Zahradnikova et al. 1999) suggest that RyRs can respond rapidly to calcium influx via DHPRs; the responsiveness of RyRs *in situ* depends on the geometrical arrangement of channels in the narrow dyadic space, in which high Ca^{2+} levels rapidly develop near the SR membrane. Such high Ca^{2+} levels lead to a rapid rate of binding of calcium to the RyR calcium sensitive sites, thereby reducing the latency between DHPR opening and SR calcium release to ~1 ms, in correspondence with the experimentally observed DHPR mean open times. However, direct measurements of the latency between long (~20-ms) calcium channel openings and spark activation (Wang et al. 2001) indicated a much longer latency (~7 ms). Since the binding of Mg^{2+} (Zahradnikova et al. 2010, Zahradnikova et al. 2003) has not been included in the model (Cannell and Soeller 1997), it may be inferred that only RyR channels that do not have Mg^{2+} bound are able to respond rapidly to DHPR openings (Zahradnikova et al. 2010, Zahradnikova et al. 2003).

It is not clear how many RyR channels contribute to a Ca^{2+} spark. While there are 5-9 RyRs per DHPR in cardiac myocytes, individual Ca^{2+} sparks may reflect activation of up to 20 RyRs (Bridge et al. 1999, Lukyanenko et al. 2000). This means that the majority of RyRs are activated by neighbouring RyRs and not by adjacent DHPR channels. A quantitative model of spark activation based on the allosteric action of Ca^{2+} and Mg^{2+} on RyR2 opening (Zahradnikova et al. 2010) predicts the opening of 1–8 RyR2 channels per spark, in agreement with experimental findings (Wang et al. 2001).

3. Structure of ryanodine receptors

3.1 Overall structural features determined by cryoelectron microscopy (cryo-EM)

RyR channels are the largest ion channels known so far, which makes structural studies of them very challenging. So far, the structure of a whole RyR has been determined only by cryo-EM. Most of these studies, including sub-nanometer EM (Samso et al. 2009,

Serysheva et al. 2008) have focused on the skeletal RyR1 isoform, but some studies have been performed on RyR2 (Liu et al. 2002, Sharma et al. 1998) and RyR3 (Liu et al. 2001, Sharma et al. 2000) as well. In agreement with the high sequence homology of RyRs, which reaches ~65%, EM structures of all three isoforms are very similar (Wagenknecht and Samso 2002). The RyR2 (Sharma et al. 1998) and RyR3 (Sharma et al. 2000) isoforms differ slightly from the RyR1 isoform in several structural domains (called divergent regions) that map to segments of reduced homology between the RyR isoforms (Zhang et al. 2003), though the overall structure of the RyR isoforms is very well conserved (Wagenknecht and Samso 2002). The complete channel is made from a combination of four monomers to yield a tetramer with a fourfold axis of symmetry. The divergent regions have been suggested to play a role in calcium-dependent inactivation (DR1) (Du and Maclennan 1999), in signal transmission between DHPR and RyR1 (DR2) (Perez et al. 2003), and in conformational changes of the RyR and RyR-RyR interactions (DR3) (Zhang et al. 2003).

Each subunit of the RyR homotetramer consists of two main parts: a cytoplasmic part and a transmembrane part. The cytoplasmic part of the whole receptor, also called the "foot", is very large (280 × 280 × 120 Å) and interacts with many modulators which affect channel gating (Yano et al. 2006). It is composed of several structural segments: the clamp and the handle at the perimeter, the central rim surrounding the putative pore, and the column connecting the cytoplasmic and transmembrane parts (Fig. 1). These segments have been further subdivided into 15 subdomains (Lanner et al. 2010). The clamps are located at the corners of the cytoplasmic part and are likely to participate in intermolecular interactions with neighboring RyR molecules and other RyR modulators. They undergo large changes during the opening and closing of the channel (Orlova et al. 1996, Samso et al. 2009, Serysheva et al. 1999). Like the cytoplasmic domain, the transmembrane part undergoes large structural changes during the opening and closing of the RyR2 channel (Orlova et al. 1996, Samso et al. 2009, Serysheva et al. 1999).

3.2 Bioinformatics domain prediction

To find the putative individual structural entities of hRyR2, we analyzed the whole hRyR2 amino acid sequence using the PFAM domain database (Finn et al. 2008). Fourteen probable domains were found in the hRyR2 monomer. Eight of them are located in the N-terminal region (residues 1–~1561) and were identified as Ins145_P3_rec, MIR, RIH, SPRY and two RyR domains. The central region (residues 1562–3000) contains the RIH domain and two RyR domains. The C-terminal part (residues 3001–4995) contains an RIH associated domain, a RR_TM4-6 domain and an Ion_Trans domain, Fig. 2. The beginnings and ends of each domain are numbered according to the PFAM search results. Mutations of specific residues involved in ARVD2 and CPVT1 are shown (Yano et al. 2006; www.fsm.it/cardmoc). LIZ1-3 (amino acid residues 554–585, 1603–1631, and 3003–3039) represent leucine-isoleucine zipper areas. The proposed binding partners, SPI, PR130, mKAP, PP1, PP2A, PKA, D, K201, FKBP, and CaM represent spinophilin, protein 130, muscle specific kinase anchoring protein, protein phosphatases 1 and 2A, protein kinase A, dantrolene, 1,4-benzothiazepine derivative K201 (JTV519), FK-binding protein, and calmodulin, respectively. Binding partners for hRyR2 and their positions were adapted from Wang et al. (2011), Yamamoto et al. (2008), and Yano et al. (2006).
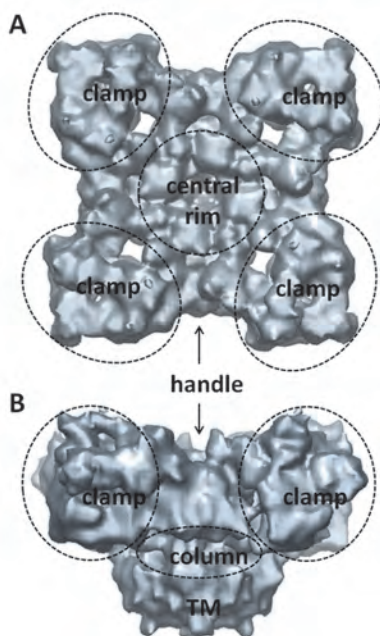
Fig. 1. A cryo-EM density map of RyR1 (accession no. 1274, http://www.ebi.ac.uk/emdb-srv/atlas/1274_summary.html) in the in closed state. A. Cytopasmic view. B. Side view. The cytoplasmic (clamp, handle, central rim and column) and transmembrane regions (TM) are indicated.
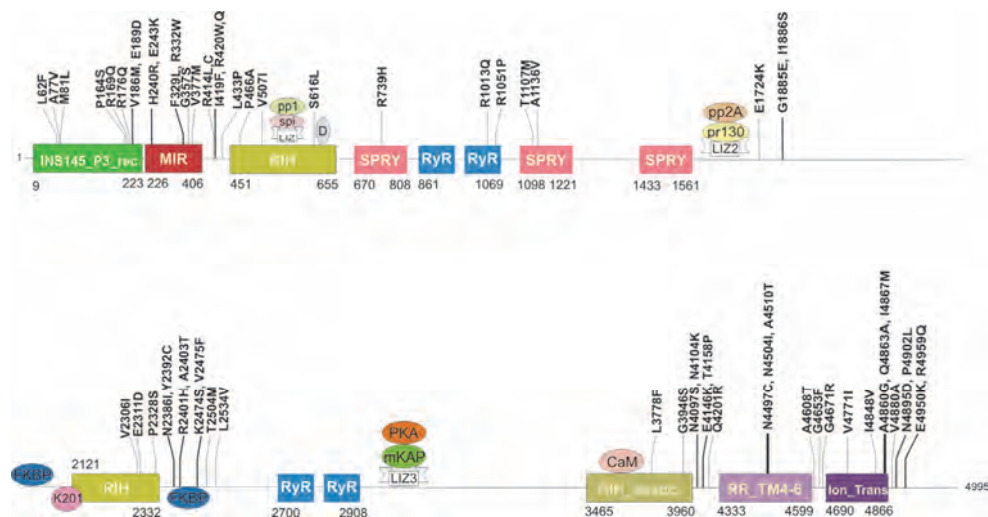

Fig. 2. Analysis of the human cardiac ryanodine receptor using the PFAM database. The position and type of mutations resulting in CVPT or ARVD2, as reported at www.fsm.it/cardmoc/, are indicated above the sequence regions.

3.3 X-ray analysis

To date, X-ray structures have been determined for several N-terminal fragments of rabbit RyR1 (residues ~12–210 (Amador et al. 2009, Lobo and Van Petegem 2009); residues 12–532 (Tung et al. 2010)); and murine RyR2 (residues 12–217, wt and mutants A77V and V186M) (Lobo and Van Petegem 2009). The overall structures of all isoforms, including those containing mutations, are very similar (superposition results in r.m.s.d. of 0.69 Å for 150 C_α atoms), Fig. 3, which is not surprising due to their close sequence homology and physiological function. The longest fragment, residues 12–532, is composed of three structural domains, which have been designated as A (1–205), B (206–394) and C (395–532) (Tung et al. 2010). Domains B and C are homologous respectively with the β-trefoil and α-helical domains of the IP3R binding core. Domain A is homologous with the IP3 binding suppressor domain of IP3R (Yuchi and Van Petegem 2011). The central motif of domains A and B is a β-trefoil core consisting of 12 β-strands which are held together by hydrophobic interactions. In the A domain, a 10-residue α-helix is inserted between strands β4 and β5 (Lobo and Van Petegem 2009). Domain C consists of five α-helices. Most of the secondary structure elements are connected by flexible loops, which were proposed to be located at the interfaces with other RyR domains or at the interfaces with proteins interacting with RyR (Tung et al. 2010, Yano et al. 2006). The X-ray crystal structures allowed the precise mapping of several mutations which are associated with CPVT and ARVD2 (Lobo and Van Petegem 2009), as well as the homologous mutations in RyR1 which are responsible for malignant hyperthermia (MH) and central core disease (CCD) (Tung et al. 2010).
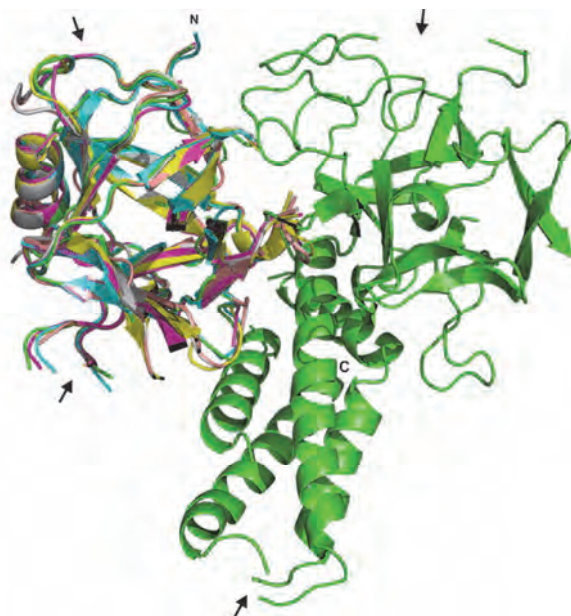

Fig. 3. Comparison of X-ray structures of the N-terminal domains of RyR1 (PDB ID 2XOA green, 3HSM pink, 3ILA magenta) and RyR2 (PDB ID 3IM5 blue, 3IM6 yellow, 3IM7 purple). The superposition was performed using the program Multiprot (Shatsky et al. 2004), through 150 C_α atoms with a r.m.s.d. of 0.69 Å. Arrows indicate flexible loops.

3.4 Relationships between domain structure, 3D structure and RyR function
3.4.1 The Ins145_P3_rec domain

The Ins145_P3_rec domain is found in RyRs and IP3Rs (Ponting C. P. 2000). In IP3R, it participates in forming the ligand binding suppressor region (Bosanac et al. 2005). In the structure of RyR1, it is equivalent to the first N-terminal domain A (Tung et al. 2010). The PFAM prediction assigned this domain to residues 9–223, while in the RyR1 structure it corresponds to the equivalent RyR2 amino acids 12–228. This domain contains two closely spaced clusters of mutations associated with CPVT and ARVD in the region of residues 62–81 and 164–189 (http://www.fsm.it/cardmoc), which belong to the first mutation cluster CPVT-I (George et al. 2007). The domain consists of 12 β-strands, arranged into a β-trefoil motif (see below). Superposing the ligand-binding suppressor domain of the IP3R (PDB ID 1XZZ; (Serysheva et al. 2008)) and the X-ray structure of the N-terminal portion of RyR1 into the cryo-EM density map of RyR1 (Tung et al. 2010) indicates that this domain should lie in the clamp or on the central rim of the ion channel, respectively.

3.4.2 The MIR domain

MIR domains are found in a number of proteins (George et al. 2007, Hamada et al. 1996, Strahl-Bolsinger and Scheinost 1999), including IP3Rs (Bosanac et al. 2005, Bosanac et al. 2002), and RyRs (Amador et al. 2009, Lobo and Van Petegem 2009, Ponting 2000, Tung et al. 2010). They usually consist of several ~50-residue MIR motifs with a β-trefoil fold (Murzin et al. 1992), and form β-barrel structures with hairpin triplets and internal pseudo-threefold symmetry (Bosanac et al. 2005). In RyR1, the MIR domain is equivalent to the second N-terminal domain, domain B (Tung et al. 2010). In PMT1 mannosyltransferases, MIR motifs are located in the luminal loops of the enzyme and are essential for transferase activity (Stahl-Bolsinger et al., 1999). In IP3R, the first two of the β-trefoil motifs were found to belong to the suppressor region (Ins145_P3_rec, (Bosanac et al. 2002), see above), while the latter two (parts of the MIR domain) belong to the ligand binding region (Bosanac et al. 2005). Similar β-trefoil motifs were predicted to be present in the N-terminal region of the RyR1 isoform (Bosanac et al. 2002), and were later found in its crystal structure (Amador et al. 2009), although the sequence similarity between IP3R and RyR is relatively low. PFAM predicted this domain to lie between residues 226–406 of RyR2, and in the RyR1 structure it corresponds to the equivalent RyR2 amino acids 228–411. This region contains a large number of CPVT/ARVD2 mutations (Fig. 2) (http://www.fsm.it/cardmoc/), which belong to the first mutation cluster CPVT-I (George et al. 2007). Docking of the ligand-binding domain of IP3R (PDB ID 1N4K, (Serysheva et al. 2005); PDB ID 1XZZ and PDB ID 1N4K, (Serysheva et al. 2008)) into the cryo-EM structure of RyR1 predicts that this domain will lie in the clamp region while doing a similar docking using the X-ray structure of the N-terminal sequence of RyR1 (Tung et al. 2010) indicates that the MIR domain should lie on the central rim.

3.4.3 The RIH domains

Two RIH domains were found in both RyRs and IP3Rs. The X-ray structure of a major part of the first RIH domain of both IP3R (Bosanac et al. 2002) and RyR1 (Tung et al. 2010) has been determined. In the case of RyR1, this corresponds to domain C and the structure extends out to residue 532, which corresponds to residue 543 in hRyR2. Structurally, RIH is composed of α-helices. In IP3R, this domain forms the binding site for inositol 1,4,5-

trisphosphate (Bosanac et al. 2002). By superposing the ligand suppressor domain (PDB ID 1XZZ) and the ligand binding core (PDB ID 1N4K) on the N-terminal part of RyR1 (PDB ID 2XAO), it was proposed that all three domains of IP3R, i.e. Ins145_P3_rec, MIR and RIH, interact together, as predicted by Chan et al. (2007), and are arranged similarly as in the N-terminal part of RyR1 (Yuchi and Van Petegem 2011). The PFAM prediction placed this domain between residues 451–655, while in the RyR1 structure its beginning corresponds to the equivalent RyR2 amino acid 410. In RyR2, the RIH domain was reported to contain a leucine–isoleucine zipper between amino acid residues 554 and 585 that mediates binding of the phosphatase PP1 via the spinophilin targeting protein (Marx et al. 2001). This domain was also proposed to contain the binding site for dantrolene (residue 626 in hRyR2), and it contains several of the CPVT/ARVD2 mutations (http://www.fsm.it/cardmoc/), which belong to the first mutation cluster CPVT-I (George et al. 2007). It was located in the clamp region by cryo-EM (Wang et al. 2011). However, docking of the X-ray structure of the N-terminal sequence of RyR1 into the cryo-EM structure of RyR1 predicts that this domain lies in the central rim (Tung et al. 2010).

PFAM predicted that the second RIH domain lies between residues 2121-2332. This domain and its C-terminally adjacent region contain the central cluster of CPVT/ARVD mutations (CPVT-II, (George et al. 2007), http://www.fsm.it/cardmoc/) and is flanked by putative binding sites for the protein FKBP 12.6. Cryo-EM places this region in the clamp (Liu et al. 2005, Wang et al. 2011).

3.4.4 The SPRY domains

The SPRY domain (**sp**1A kinase and the **ry**anodine receptors) (Ponting et al. 1997) structurally consists of several antiparallel β-strands connected with flexible loops. The precise function of the SPRY domain (and the related B30.2 domain) is unknown; however, it is believed to act as a protein–protein interaction module capable of binding multiple targets by recognizing the conformation of a partner protein rather than a consensus sequence motif (Woo et al. 2006, Yao et al. 2006). The B30.2/SPRY domain has been identified in numerous and diverse proteins across bacterial and eukaryotic species (e.g. pyrin/marenostrin and other butyrophilin-like homologues, ryanodine receptors and midin1), including over 150 proteins in humans (Rhodes et al. 2005), suggesting that the specific function of the B30.2/SPRY domain within a given protein may heavily rely on the other domains in their neighbourhood (Kleiber and Singh 2009). PFAM predicted that RyR2 contains three SPRY domains, corresponding to residues 670–808, 1098–1221, and 1433–1561. The first two domains contain three CPVT/ARVD mutations: R739H, T1107M and A1136V (Medeiros-Domingo et al. 2009), Fig. 2, which lie outside of the four mutation clusters.

3.4.5 The RyR domains

Four copies of the RyR domain are present in the ryanodine receptor, of which two belong to the N-terminal and two to the central regions. The function of this domain is unknown (Ponting 2000). In the second RyR domain, two isolated CPVT mutations, which lie outside of the four mutation clusters, have been found to date: R1013Q and R1051P, Fig. 2 (Marjamaa et al. 2009, Medeiros-Domingo et al. 2009).

3.4.6 The RIH_associated and RR_TM4-6 domains

According to PFAM, the RIH_associated domain should lie between residues 3465–3960. This domain contains the calmodulin binding site, which was localized to the column region

of RyR according to cryo-EM (Samso and Wagenknecht 2002). The adjacent RR_TM4-6 domain was predicted to lie between residues 4333–4599 by PFAM. It contains the divergent region DR1 (Liu et al. 2002), the putative calcium sensor that is responsible for the physiological activation of RyR2 (Chen et al. 1998, Li and Chen 2001), and also the calmodulin-like domain (Xiong et al. 2006). The end of the RIH_associated domain together with the RR_TM4-6 domain (aa. 3722–4610) were identified as a separate functional domain (called the I-domain) (George et al. 2004), which contains a third cluster of CPVT/ARVD mutations (CPVT-III, (George et al. 2007), http://www.fsm.it/cardmoc/); cryo-EM locates this domain in the column of RyR1 (Wang et al. 2011).

3.4.7 The Ion_Trans domain

The Ion_Trans (ion transport) domain covers the transmembrane region of the ryanodine receptor. This domain is found in most voltage-dependent ion channels as well as in RyRs and IP3Rs. The domain usually has six transmembrane helices, the final two of which flank a loop that determines ion selectivity (Unnerstale et al. 2009). The tetrameric ion channels (potassium channels, IP3Rs and RyRs) contain one Ion_Trans domain per monomer, while the sodium and calcium channels contain four Ion_Trans domain repeats. This domain is located in the transmembrane region, embedded in the membrane of the SR, Fig. 1A,B, and contains the ion conducting pore. It has been proposed that the pore includes the GVRAGGGIGD amino acid sequence (Du et al. 2001, Zhao et al. 1999), where the amino acids GGIG were proposed to form a selectivity filter (Balshaw et al. 1999, Gao et al. 2000). The fourth cluster of CPVT/ARVD2 mutations (CPVT-IV, (George et al. 2007), http://www.fsm.it/cardmoc/) occurs in this domain and in the flanking regions on both its sides.

3.4.8 Regions without a known domain structure

Two of the three regions of isoform sequence diversity (DR2 and DR3; (Perez et al. 2003, Zhang et al. 2003)) are located outside of the PFAM-predicted domains. DR2 is located between the second and the third SPRY domains (residues 1353-1397, Liu et al. 2004), while DR3 (residues 1852-1890) is located between SPRY3 and RIH2. Both DR2 and DR3 are found in the clamp region of RyR1 (Wang et al. 2011). DR3 contains two isolated CPVT/ARVD2 mutations, G1885E and G1886S (Milting et al. 2006), which lie outside of the four mutation clusters.

The second and third leucine-isoleucine zipper (aa. 1604–1644 and 3004–3041), that were found to bind PP2A and PKA with the help of the adapter proteins PR130 and mAKAP, respectively (Marx et al. 2001), are also located outside the PFAM-predicted domains. The location of these motifs in the 3D structure of the RyR2 is unknown.

4. Cloning, expression and characterization of predicted N-terminal hRyR2 domains

In our previous work we concentrated on the production and characterization of recombinant N-terminal domains of hRyR2 (residues 1–759) in *Escherichia coli* expression systems ((Bauerova-Hlinkova et al. 2010); unpublished results). Based on the bioinformatics analysis described above, we assumed that the predicted domains would form individual entities and might behave as stable proteins. We designed several constructs covering the

predicted first three N-terminal domains (Ins145_P3_rec, MIR, RIH) with various starting and terminating residues, Table 1, taking into consideration the predicted secondary structure elements and the known structure of the related IP3R domains. All fragments were designed not to disrupt the predicted secondary structure elements, Fig. 6. In this study we obtained three authentic recombinant hRyR2 fragments with good expression yields and solubility: 1–606 (involves first three putative N-terminal domains), 391–606 and 409–606 (involves the core of the predicted RIH domain) and several hRyR2 fragments expressed with a fusion partner, either thioredoxin or Nus A protein, Table 1.

hRyR2 fragment	Calculated $M_w \times 10^3$	Protein Expression
1–247.His$_6$	27.9	++
1–606.His$_6$	68.6	++
391–606.His$_6$	25.2	++
409–606.His$_6$	23.2	+++
Nus.1–606	128.6	++
Nus.230–606	104.0	++
Trx.384–606.His$_6$	43.3	+++
Trx.391–606.His$_6$	42.5	+++
Trx.409–606.His$_6$	40.5	+++

Table 1. Designed fragments of the N-terminal part of hRyR2 with good expression and solubility. The fragment 1–247.His6 contains the Ins145_P3_rec domain. The longest N-terminal hRyR2 fragment 1–606.His6 involves all three putative N-terminal domains. The hRyR fragments 384–606, 391–606 and 409–606 involve the core of the RIH domain. To improve solubility, some fragments were expressed with fusion partners – Nus A protein and thioredoxin. Quantification of expression: ++ 1–5 mg/g expressed cells, +++ more than 5 mg/g expressed cells. The amount of the protein was determined after IMAC purification (Bauerova-Hlinkova et al. 2010).

The folding and thermal stability of these expressed fragments was assessed by circular dichroism (CD) spectroscopy (Fig. 4) and a thermofluor shift assay (Fig. 5). The secondary structure content of the fragments was derived from the CD spectra using the CDsstr algorithm (Johnson 1999) with an extensive set of reference databases (Whitmore and Wallace 2004). For the longest fragment, 1–606, the amount of α-helices and β-strands resulted in *ca.* 23 and 29%, respectively (Fig. 4A; (Bauerova-Hlinkova et al. 2010). For the C-terminal domain covering residues 409 to 606 (Fig. 4B), a higher degree of α-helicity (*ca.* 50%) was found. This value is lower than expected from the model for this region (62%, see section 4.1.), which indicates that the expected N-terminal helix might be only partially folded. Such disorder within the terminal regions is frequently observed in NMR and X-ray derived structures of protein fragments. The spectra of the thioredoxin fusion protein fragments 384–606 (Fig. 4C) and 409–606 (Fig. 4D) indicated α-helix and β-strand contents of *ca.* 40 and 10%, respectively.

With temperature increasing up to 35°C, only small changes of the CD signal could be observed for fragment 1–606 (Fig. 5A), but further heating resulted in irreversible precipitation under our experimental conditions (Bauerova-Hlinkova et al. 2010). A similar behaviour was observed for the fragment 409–606, which was stable up to 37°C (Fig. 4B) and started to precipitate at T > 42°C (data not shown). When the fragment 409–606 was fused

with thioredoxin A, its CD signal indicated a gradual loss of α-helicity (*ca.* 25% at 95°C) that was fully recovered upon cooling (data not shown).
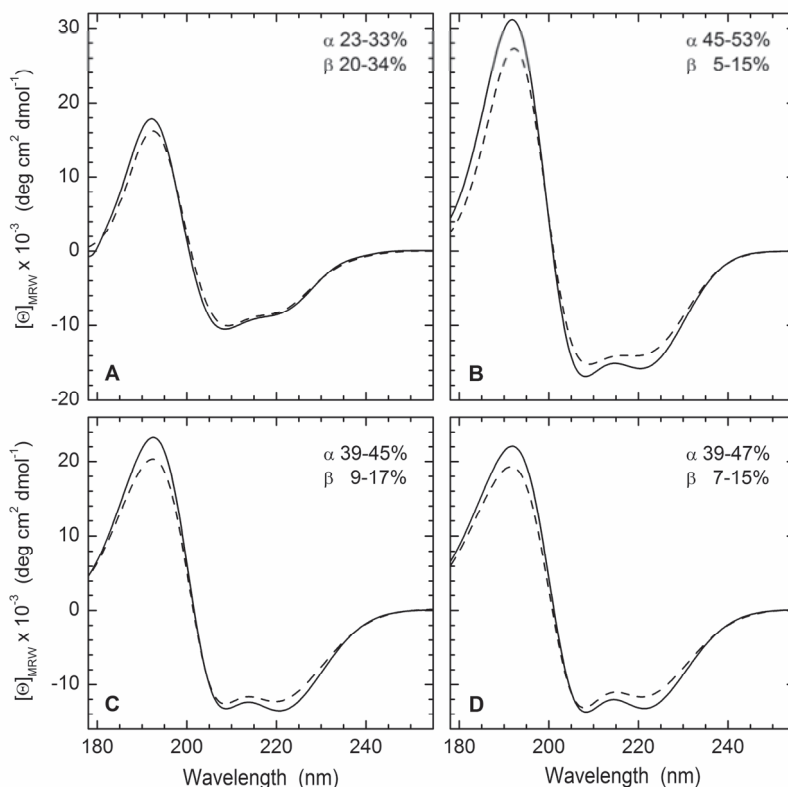

Fig. 4. Far-UV CD spectra of recombinant hRyR2 fragments 1–606 (A) and 409-606 (B), and as fusion proteins with thioredoxin A at the N-terminus Trx-384-606 (C) and Trx-409-606 (D). Spectra were recorded in an 0.02-cm cell at 4°C (solid line) and 37°C (dashed line; 35°C for hRyR2 1–606). Samples were dialyzed into 100 mM NaF, 20 mM Tris SO$_4$ pH 7.5 or 8.0, including either 0.1% Tween-20 (A-C) or sulfobetaine SB14 (D). Deconvolution of the 4°C spectra using the CDsstr algorithm as implemented in Dichroweb with various reference databases ((Whitmore and Wallace 2004); http://dichroweb.cryst.bbk.ac.uk/) results in the amount of α-helix and β-strand shown at the top right of each panel.

The results of the thermofluor shift assay, performed with the longest hRyR2 fragment 1–606, were in good agreement with the temperature dependence of the circular dichroism spectra. The thermal stability of the fragment was tested in a wide range of buffers (Tris, Hepes, MES, citrate, Na/K phosphate, Bicine, Tricine; pH range 5.0–9.0), Fig. 5, and in the presence or absence of 1 and 5 mM Ca^{2+}, Mg^{2+}, ATP and 5–20% glycerol. The fragment is the most stable in neutral-basic pH (7.0–8.0) with a T_m of ~45°C, Fig. 5B, C. The presence of Ca^{2+}

or ATP did not change the T_m significantly, suggesting that the fragment does not contain binding sites for these ligands.
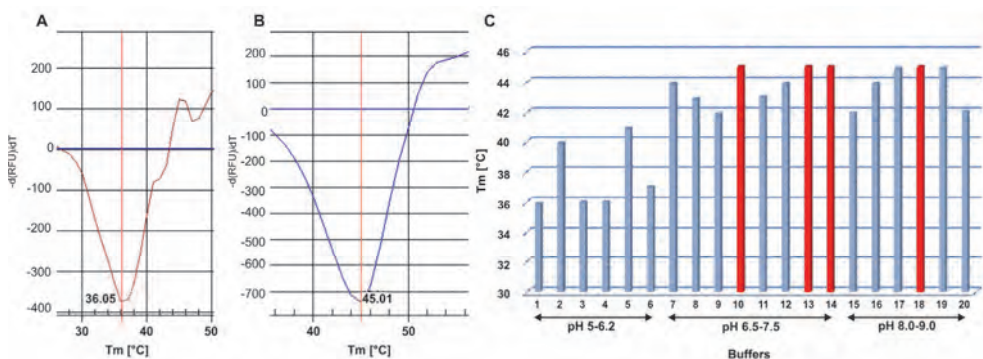

Fig. 5. The first derivative of the thermal denaturation curve of recombinant 1–606 hRyR2 fragment obtained by thermofluor shift assay, measured in 200 mM Na-citrate, pH 5.5 (A), and 200 mM Na-phosphate, pH 7.5 (B). C. T_m of the recombinant hRyR2 fragment 1-606 obtained by the thermofluor shift assay in different buffers and pH (1 – K-phosphate 5.0; 2 – Na-phosphate 5.5; 3 – Na-citrate 5.5; 4 – MES 5.8; 5 – K-phosphate 6.0; 6 – MES 6.2; 7 – Na-phosphate 6.5; 8 – Na-cacodylate 6.5; 9 – MES 6.5; 10 – K-phosphate 7.0; 11 – HEPES 7.0; 12 – Na-acetate 7.3; 13 – Na-phosphate 7.5; 14 – Tris 7.5; 15 – Imidazol 8.0; 16 – HEPES 8.0; 17 – Tris 8.0; 18 – Bicine 8.0; 19 – Tris 8.5; 20 – Bicine 9.0). The conditions under which RyR2 1–606 was the most stable are in red. For each measurement 8 µg of protein were used.

4.1 Model structure of the N-terminal part of hRyR2

The amino-acid sequence of the recently determined structure of the N-terminal region of rabbit RyR1 (PDB ID 2XOA (Tung et al. 2010)) is 63% identical and 77% similar to the corresponding sequence of hRyR2 (similarity is here defined as having a Gonnet Pam250 matrix score > 0.5 as determined by ClustalX 2.1). The 2XOA structure therefore represents an excellent template for constructing a homology model of the N-terminal region of hRyR2. The structure covers residues 12–543 of the hRyR2 sequence. The homology model was constructed using Modeller 9v8 (Sali and Blundell 1993). The hRyR2 sequence was first aligned with the template structure using the alignment.align2d command of Modeller and then manually edited to improve the alignment (Fig. 6). This alignment was used to build a homology model using the automodel class. Residues 90–107 of the human sequence, which had been disordered in the template structure, were constrained to form an α-helix in accordance with the secondary structure predictions, see below. The structure was thoroughly refined using automodel.library_schedule = autosched.slow and automodel.max_var_iterations = 300 for the initial optimization step, which was then followed by molecular dynamics refinement using automodel.md_level = refine.slow. The whole process was repeated twice. The refinement target function (objective function) minimized the geometry restraints and Charmm energy terms enforcing proper stereochemistry (described in (Sali and Blundell 1993)).

```
            β1           β2              β3        3₁₀   β4    α1
      10        20        30        40        50        60        70
RyR1  MGDGGEGEDEVQFLRTDDEVVLQCSATVLKEQLKLCLAAEGFGNRLCFLEPTSNAQNVPPDLAICCFTLEQSLSVRALQ
RyR2  MADGGEGEDEIQFLRTDDEVVLQCTATIHKEQQKLCLAAEGFGNRLCFLESTSNSKNVPPDLSICTFVLEQSLSVRALQ
      * ******** ************* ** *** ****************** *** ****** ** * ***********
          β1A      β1          β2        β3              β4

                                        β5        β6              β7
      80        90       100       110       120       130       140       150
RyR1  EMLANTVEAGVES-----------SQGGGHRTLLYGHAILLRHAHSRMYLSCLTTSRSMTDKLAFDVGLQEDATGEAC
RyR2  EMLANTVEKSEGQVDVEKWKFMMKTAQGGGHRTLLYGHAILLRHSYSGMYLCCLSTSRSSTDKLAFDVGLQEDTTGEAC
      ********            ****************** * *** ** **** *************** *****
              α1              β5A     β5       β6              β7

        β8              β9        β10      β11        β12              β13
      160       170       180       190       200       210       220       230
RyR1  WWTMHPASKQRSEGEKVRVGDDLILVSVSSERYLHLSTASGELQVDASFMQTLWNMNPICSCCE--EGYVTGGHVLRLF
RyR2  WWTIHPASKQRSEGEKVRVGDDLILVSVSSERYLHLSYGNGSLHVDAAFQQTLWSVAPISSGSEAAQGYLIGGDVLRLL
      ***** ******** ********************* * * ***** **** ** * ** ** ****
        β8            β9A  β9                    β11       β12        β13A  β13

        β14             β15    3₁₀    3₁₀    β16               β17    β18    β19
      240       250       260       270       280       290       300       310
RyR1  HGHMDECLTISAAD-SDDQRRLVYYEGGAVCTHARSLWRLEPLRISWSGSHLRWGQPLRIRHVTTGRYLALTEDQGLVVVD
RyR2  HGHMDECLTVPSGEHGEEQRRTVHYEGGAVSVHARSLWRLETLRVAWSGSHIRWGQPFRLRHVTTGKYLSLMEDKNLLLMD
      ********* ***** ****** ************* *********** * ****** ** * ** * *
        β14            β15           β16                  β17    β18    β19

      3₁₀   α    β20                       β21      β22              β23
      320       330       340       350       360       370       380       390
RyR1  ACKAHTKATSFCFRVSKEKLDTAPKRDVEGMGPPEIKYGESLCFVQHVASGLWLTYAAPDPKALRLGVLKKKAILHQEGHM
RyR2  KEKADVKSTAFTFRSSKEKLDVGVRKEVDGMGTSEIKYGDSVCYIQHVDTGLWLTYQSVDVKSVRMGSIQRKAIMHHEGHM
      ** * * ** ********* *** ***** *** *** ****** * * ***** ****
                   β20              β21      β22

        β24           α2                         α3
      400       410       420       430       440       450       460       470
RyR1  DDALFLTRCQQEESQAARMIHSTAGLYNQFIKGLDSFSGKPRGSGPPAGPALPIEAVILSLQDLIGYFEPPSEELQHEEKQ
RyR2  DDGISLSRSQHEESRTARVIRSTVFLFNRFIRGLDALSKKAKAS----TVDLPIESVSLSLQDLIGYFHPPDEHLEHEDKQ
      ** * *** *** ** * * * ** ** ** * **** * ************* * * ** **
        β24           α2                         α3

        α4           α5            3₁₀   α6
      480       490       500       510       520       530       540
RyR1  SKLRSLRNRQSLFQEEGMLSLVLNCIDRLNVYTTAAHFAEYAGEEAAESWKEIVNLLYELLASLIRG
RyR2  NRLRALKNRQNLFQEEGMINLVLECIDRLHVYSSAAHFADVAGREAGESWKSILNSLYELLAALIRG
      ** * *** ******** ********* ** ***** ** ** **** * ***********
              α4(5)                      3₁₀    α6
```
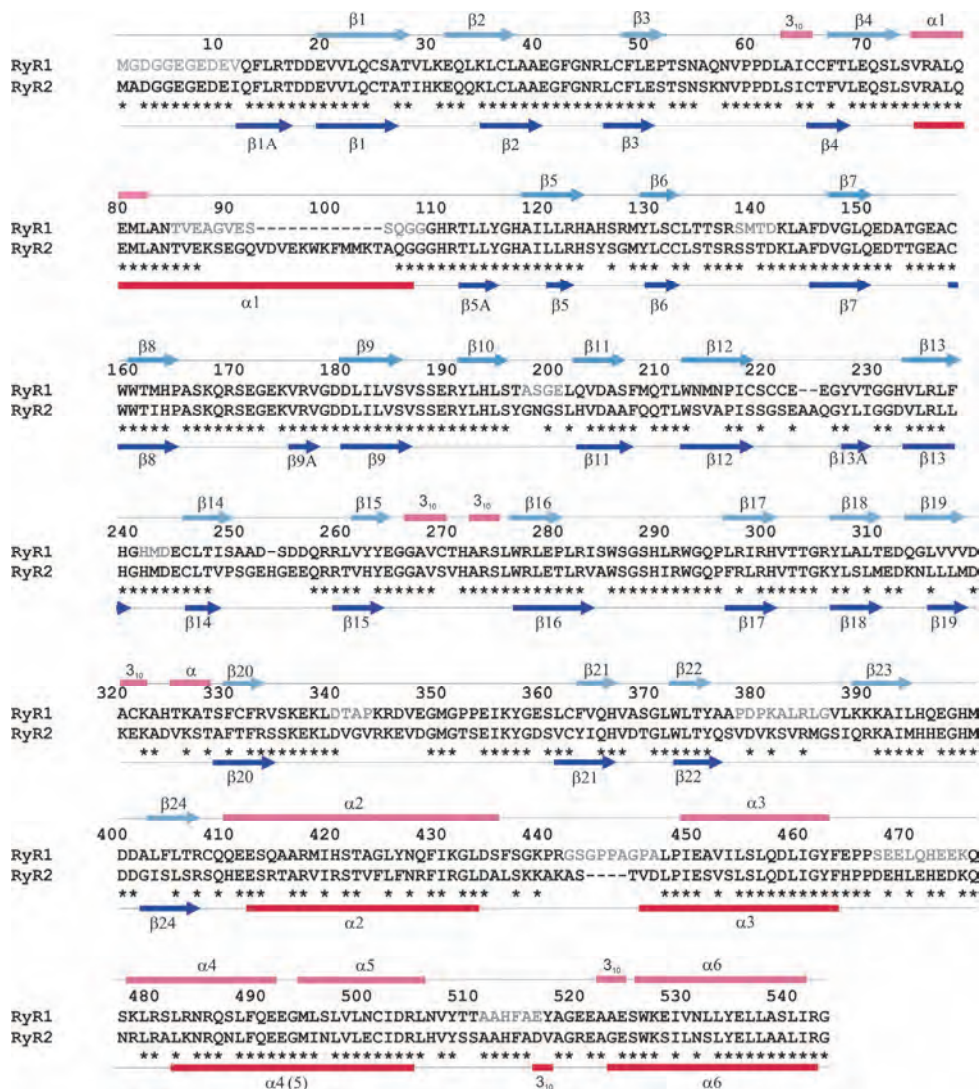
Fig. 6. The sequence alignment of hRyR2 and rabbit RyR1 (PDB ID 2XOA) sequences which was used as a template for the homology modeling of the hRyR2 tertiary structure. The alignment was performed using the alignment.align2d command of Modeller 9v8 (Sali and Blundell 1993). The secondary structure elements of hRyR2 (α-helices and β-strands are shown as red bars and blue arrows, respectively) were predicted by Jpred (Cole et al. 2008). The numbering of predicted secondary structure elements of hRyR2 corresponds to those found in the RyR1 template structure (α-helices and β-strands are shown as pink bars and light blue arrows, respectively). The alignment covers residues 1–543 of the human RyR2 protein. Residues in grey are missing in the RyR1 structure and correspond to flexible loops. Identical residues (~64%) in both sequences are labelled by asterisks.

Twenty trial structures were generated and the best one was chosen by first discarding all those with unreasonable geometry in the loop regions, and then selecting the one with the lowest objective function score. The loops in this structure were then refined using the functions found in the Modeller loopmodel class (described in Fiser et al. (2000)). This was done in two stages. First, the loop containing helix α1A (see below) was refined to give five different positions. Second, for each of these positions an additional five structures were generated with different positions for all of the loops. The final structure was selected based on the lowest objective function. The final structure was inserted into the RyR1 crystal packing arrangement to check for possible clashes with neighbouring molecules, which might indicate unlikely loop conformations; none were found. The final model is shown in Fig. 7A,B.

The hRyR2 model contains three domains, aa. 12–219 (Ins145_P3_rec), 228–408 (MIR) and 411–543 (RIH; residue numbers refer to the hRyR2), analogous to those of the template structure (Tung et al. 2010). The RyR1 template structure and hRyR2 homology model are in agreement with the PFAM predictions shown in Fig. 2; however, the beginning of the third domain, RIH, is shifted by about 40 aa. residues towards the N-terminus.

With a few exceptions, the hRyR2 homology model (Fig. 7) confirmed the secondary structure predictions, nearly all of the β-strands (22 out of 27) were found in the predicted positions in the template structure, although with a minor shift of one to three residues, Fig. 6.
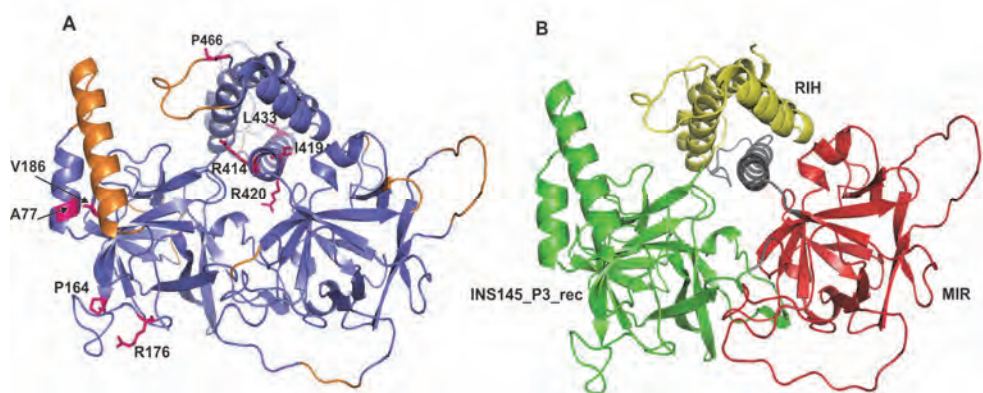

Fig. 7. (A) hRyR2 homology model constructed by Modeller 9v8 (Sali and Blundell 1993) using the alignment with rabbit RyR1, shown in Fig. 6. Loops which were disordered in the template structure and the modelled α1A-helix are in orange. Residues which cause physiological dysfunction of hRyR2 when mutated are indicated. (B) The RyR2 homology model coloured according to the domains predicted using the PFAM database. The colour scheme is the same as in Fig. 2; Ins145_P3_rec is green, MIR is red, and RIH is yellow. The grey α-helix, α2 (aa. 409–436), according to the PFAM results, precedes the RIH domain, but is not part of the MIR domain.

The beginning of the first β-strand (β1A; aa. 11–16) was missing in the template structure so that its presence could not be verified. The short β-strands β5A, β9A, and β13A were not present in the RyR1 structure. β23 was present in the template and the modelled structure but was not predicted by JPred. Three long α-helices (α2, α3, and α6) were correctly

predicted by JPred with small variations at the beginnings or the ends in the model. In the region of the predicted helix α4, two shorter α-helices were modelled which are separated from each other only by a two-residue turn, as found in the template structure. Neither the shortest α-helix (aa. 325–328) nor four out of the five 3_{10} helices were predicted.

The first predicted α-helix (α1) deserves additional consideration. In comparison to RyR1, the RyR2 sequence contains a 12-residue insertion, Fig. 6, suggesting that the structure of this region differs in these two proteins. In hRyR2, helix α1 was predicted to be 33 residues long (residues 75–107). However, the Ins145_P3_rec domain, which includes the helix α1, was determined independently three times in RyR2 and contains only the first ten residues of this helix, followed by a gap (Lobo and Van Petegem 2009). This indicates that the predicted helix α1 cannot span the whole range. Instead, most likely, this region forms a helix-turn-helix motif (aa. 75–110), as found in the structure of the IP3R ligand binding suppressor domain (Bosanac et al. 2005). The motif has to be rather flexible to explain its absence in the previously solved RyR structures as well as the conformational flexibility predicted by (Bosanac et al. 2005). Inclusion of an 18-residue α1A, separated from the helix α1 observed in the template structure by a six-residue linker, resulted in five different conformations, which shows that the modelled motif has sufficient mobility to explain its absence in the solved structures. Most likely, this motif will be stabilized in the whole RyR2 protein by interaction with a binding partner (another RyR2 domain or an interacting ligand).

Between the helix α1A and the long disordered loop containing residues 464–477, there is a very large cavity, which suggests the existence of a large binding pocket. The helix α1A and the loop 464–477, which sit atop of this cavity, both contain several aromatic residues (W98, F100, H469, H472). The presence of the aromatic residues in the surface, three of which are exposed to the cavity (F100, H469, H472) may indicate protein-protein binding events with a putative ligand. The P466A mutant, located at the beginning of the loop, is known to substantially disrupt the proper physiological function of RyR2, causing syncope (Tester et al. 2005). Proline residues have lower conformational flexibility than other residues, so the most likely reason for the importance of P466 would be a necessity to decrease the flexibility of the loop containing residues 464–477. In addition to the P466A mutant, two other mutants in this area are also known to cause RyR2 dysfunction: A77V, causing CPVT and ARVD2 (d'Amati et al. 2005), and V186M, causing CPVT (Tester et al. 2006). All three mutations in this area induce only small changes in the surface shape of the protein. Taken together, all this implies that this part of the structure might be involved in the binding of RyR2 to other interacting proteins or its own domains. This is consistent with the results seen in RyR1, where the docking of the first three N-terminal domains into the full-length cryo-EM density map revealed that the loop involving P455 (P466 in hRyR2) as well as the beginning of helix α4 belong to interface 6 (Tung et al. 2010).

The reliability of the hRyR2 homology model is further confirmed by the CD-spectroscopy of hRyR2 fragment 1–606, Fig. 4A, which revealed 23% α-helices and 29% β-strands in the fragment. This is in good agreement with the hRyR2 model structure, in which the content of α-helices and β-strands was 23% and 24%, respectively.

5. Conclusion

In this work, bioinformatics analysis of the whole human RyR2 is presented. The analysis shows that the protein is composed of 14 domains. We were concerned particularly with the

first three N-terminal domains of the protein (Ins145_P3_rec, MIR, RIH). Verification that the domains identified can behave as separate, independent protein units was provided by their successful expression in *E. coli* and subsequent characterization. CD-spectroscopy was used to determine the domain organization and to identify the secondary structure elements of the N-terminal part of hRyR2. The amino acid sequence identity of hRyR2 with that of rabbit RyR1, the X-ray structure of which is known, is higher than 60%, which allowed the construction of a reliable homology model of the N-terminal part of hRyR2. Its reliability was further strengthened by its conformity with the bioinformatics analysis and the CD-spectroscopy study. This model should allow a clearer insight to be gained into the possible influence of mutations on the cardiac diseases CPVT1 and ARVD2.

6. Acknowledgment

7. References

Amador FJ, Liu S, Ishiyama N, Plevin MJ, Wilson A, MacLennan DH, Ikura M. 2009. Crystal structure of type I ryanodine receptor amino-terminal beta-trefoil domain reveals a disease-associated mutation "hot spot" loop. Proc Natl Acad Sci U S A 106: 11040-11044.

Baartscheer A, Schumacher CA, Fiolet JW. 1998. Cytoplasmic sodium, calcium and free energy change of the Na+/Ca2+-exchanger in rat ventricular myocytes. J Mol Cell Cardiol 30: 2437-2447.

Balshaw D, Gao L, Meissner G. 1999. Luminal loop of the ryanodine receptor: a pore-forming segment? Proc Natl Acad Sci U S A 96: 3345-3347.

Bauerova-Hlinkova V, Hostinova E, Gasperik J, Beck K, Borko L, Lai FA, Zahradnikova A, Sevcik J. 2010. Bioinformatic mapping and production of recombinant N-terminal domains of human cardiac ryanodine receptor 2. Protein Expr Purif 71: 33-41.

Berridge MJ. 1994. The biology and medicine of calcium signalling. Mol Cell Endocrinol 98: 119-124.

Bers DM. 2004. Macromolecular complexes regulating cardiac ryanodine receptor function. J Mol Cell Cardiol 37: 417-429.

Bhat MB, Zhao J, Takeshima H, Ma J. 1997. Functional calcium release channel formed by the carboxyl-terminal portion of ryanodine receptor. Biophys J 73: 1329-1336.

Bosanac I, Alattia JR, Mal TK, Chan J, Talarico S, Tong FK, Tong KI, Yoshikawa F, Furuichi T, Iwai M, Michikawa T, Mikoshiba K, Ikura M. 2002. Structure of the inositol 1,4,5-trisphosphate receptor binding core in complex with its ligand. Nature 420: 696-700.

Bosanac I, Yamazaki H, Matsu-Ura T, Michikawa T, Mikoshiba K, Ikura M. 2005. Crystal structure of the ligand binding suppressor domain of type 1 inositol 1,4,5-trisphosphate receptor. Mol Cell 17: 193-203.

Bridge JH, Ershler PR, Cannell MB. 1999. Properties of Ca2+ sparks evoked by action potentials in mouse ventricular myocytes. J Physiol (Lond) 518: 469-478.

Cannell MB, Soeller C. 1997. Numerical analysis of ryanodine receptor activation by L-type channel activity in the cardiac muscle diad. Biophys J 73: 112-122.

Cannell MB, Cheng H, Lederer WJ. 1994. Spatial non-uniformities in [Ca2+]i during excitation-contraction coupling in cardiac myocytes. Biophys J 67: 1942- 1956.

Cannell MB, Cheng H, Lederer WJ. 1995. The control of calcium release in heart muscle. Science 268: 1045-1049.

Chan J, Whitten AE, Jeffries CM, Bosanac I, Mal TK, Ito J, Porumb H, Michikawa T, Mikoshiba K, Trewhella J, Ikura M. 2007. Ligand-induced conformational changes via flexible linkers in the amino-terminal region of the inositol 1,4,5-trisphosphate receptor. J Mol Biol 373: 1269-1280.

Chan WM, Welch W, Sitsapesan R. 2000. Structural factors that determine the ability of adenosine and related compounds to activate the cardiac ryanodine receptor. Br J Pharmacol 130: 1618-1626.

Chan WM, Welch W, Sitsapesan R. 2003. Structural characteristics that govern binding to, and modulation through, the cardiac ryanodine receptor nucleotide binding site. Mol Pharmacol 63: 174-182.

Chen SR, Ebisawa K, Li X, Zhang L. 1998. Molecular identification of the ryanodine receptor Ca2+ sensor. J Biol Chem 273: 14675-14678.

Cheng H, Lederer WJ, Cannell MB. 1993. Calcium sparks: elementary events underlying excitation-contraction coupling in heart muscle. Science 262: 740-744.

Cheng H, Lederer MR, Lederer WJ, Cannell MB. 1996. Calcium sparks and [Ca2+]i waves in cardiac myocytes. Am J Physiol 270: C148-C159.

Chu A, Fill M, Stefani E, Entman ML. 1993. Cytoplasmic Ca2+ does not inhibit the cardiac muscle sarcoplasmic reticulum ryanodine receptor Ca2+ channel, although Ca(2+)-induced Ca2+ inactivation of Ca2+ release is observed in native vesicles. J Membr Biol 135: 49-59.

Cole C, Barber JD, Barton GJ. 2008. The Jpred 3 secondary structure prediction server. Nucleic Acids Res 36: W197-201.

Copello JA, Barg S, Sonnleitner A, Porta M, Diaz-Sylvester P, Fill M, Schindler H, Fleischer S. 2002. Differential activation by Ca2+, ATP and caffeine of cardiac and skeletal muscle ryanodine receptors after block by Mg2+. J Membr Biol 187: 51-64.

Coronado R, Morrissette J, Sukhareva M, Vaughan DM. 1994. Structure and function of ryanodine receptors. Am J Physiol 266: C1485-1504.

d'Amati G, Bagattin A, Bauce B, Rampazzo A, Autore C, Basso C, King K, Romeo MD, Gallo P, Thiene G, Danieli GA, Nava A. 2005. Juvenile sudden death in a family with polymorphic ventricular arrhythmias caused by a novel RyR2 gene mutation: evidence of specific morphological substrates. Hum Pathol 36: 761-767.

Du GG, Maclennan DH. 1999. Ca(2+) inactivation sites are located in the COOH-terminal quarter of recombinant rabbit skeletal muscle Ca(2+) release channels (ryanodine receptors). J Biol Chem 274: 26120-26126.

Du GG, Khanna VK, MacLennan DH. 2000. Mutation of divergent region 1 alters caffeine and Ca(2+) sensitivity of the skeletal muscle Ca(2+) release channel (ryanodine receptor). J Biol Chem 275: 11778-11783.

Du GG, Guo X, Khanna VK, MacLennan DH. 2001. Functional characterization of mutants in the predicted pore region of the rabbit cardiac muscle Ca(2+) release channel (ryanodine receptor isoform 2). J Biol Chem 276: 31760-31771.

Durham WJ, Wehrens XH, Sood S, Hamilton SL. 2007. Diseases associated with altered ryanodine receptor activity. Subcell Biochem 45: 273-321.

Ebashi S, Ogawa Y. 1988. Ca2+ in contractile processes. Biophys Chem 29: 137-143.

El-Hayek R, Saiki Y, Yamamoto T, Ikemoto N. 1999. A postulated role of the near amino-terminal domain of the ryanodine receptor in the regulation of the sarcoplasmic reticulum Ca(2+) channel. J Biol Chem 274: 33341-33347.

Fabiato A. 1985. Time and calcium dependence of activation and inactivation of calcium-induced release of calcium from the sarcoplasmic reticulum of a skinned canine cardiac Purkinje cell. J Gen Physiol 85: 247-289.

Faltinova A, Gaburjakova J, Zahradnikova A. 2011. Activation of the rat cardiac ryanodine receptor by its domain peptide DPcpvt-C. Physiol Res 60: *in press*.

Finn RD, Tate J, Mistry J, Coggill PC, Sammut SJ, Hotz HR, Ceric G, Forslund K, Eddy SR, Sonnhammer EL, Bateman A. 2008. The Pfam protein families database. Nucleic Acids Res 36: D281-288.

Fiser A, Do RK, Sali A. 2000. Modeling of loops in protein structures. Protein Sci 9: 1753-1773.

Gaburjakova J, Gaburjakova M. 2006. Comparison of the effects exerted by luminal Ca2+ on the sensitivity of the cardiac ryanodine receptor to caffeine and cytosolic Ca2+. J Membr Biol 212: 17-28.

Gao L, Balshaw D, Xu L, Tripathy A, Xin C, Meissner G. 2000. Evidence for a role of the lumenal M3-M4 loop in skeletal muscle Ca(2+) release channel (ryanodine receptor) activity and conductance. Biophys J 79: 828-840.

George CH, Yin CC, Lai FA. 2005. Toward a molecular understanding of the structure-function of ryanodine receptor Ca2+ release channels: perspectives from recombinant expression systems. Cell Biochem Biophys 42: 197-222.

George CH, Jundi H, Thomas NL, Fry DL, Lai FA. 2007. Ryanodine receptors and ventricular arrhythmias: emerging trends in mutations, mechanisms and therapies. J Mol Cell Cardiol 42: 34-50.

George CH, Jundi H, Thomas NL, Scoote M, Walters N, Williams AJ, Lai FA. 2004. Ryanodine receptor regulation by intramolecular interaction between cytoplasmic and transmembrane domains. Mol Biol Cell 15: 2627-2638.

Gyorke I, Gyorke S. 1998. Regulation of the cardiac ryanodine receptor channel by luminal Ca2+ involves luminal Ca2+ sensing sites. Biophys J 75: 2801-2810.

Gyorke I, Hester N, Jones LR, Gyorke S. 2004. The role of calsequestrin, triadin, and junctin in conferring cardiac ryanodine receptor responsiveness to luminal calcium. Biophys J 86: 2121-2128.

Gyorke S, Fill M. 1993. Ryanodine receptor adaptation: Control mechanism of Ca2+-induced Ca2+ release in heart. Science 260: 807-809.

Gyorke S, Velez P, Suarez-Isla B, Fill M. 1994. Activation of single cardiac and skeletal ryanodine receptor channels by flash photolysis of caged Ca2+. Biophys J 66: 1879-1886.

Hamada T, Tashiro K, Tada H, Inazawa J, Shirozu M, Shibahara K, Nakamura T, Martina N, Nakano T, Honjo T. 1996. Isolation and characterization of a novel secretory protein, stromal cell-derived factor-2 (SDF-2) using the signal sequence trap method. Gene 176: 211-214.

Ikemoto N, Yamamoto T. 2000. Postulated role of inter-domain interaction within the ryanodine receptor in Ca(2+) channel regulation. Trends Cardiovasc Med 10: 310-316.

Johnson WC. 1999. Analyzing protein circular dichroism spectra for accurate secondary structures. Proteins 35: 307-312.

Kagaya Y, Weinberg EO, Ito N, Mochizuki T, Barry WH, Lorell BH. 1995. Glycolytic inhibition: effects on diastolic relaxation and intracellular calcium handling in hypertrophied rat ventricular myocytes. J Clin Invest 95: 2766-2776.

Kettlun C, Gonzalez A, Rios E, Fill M. 2003. Unitary Ca2+ current through mammalian cardiac and amphibian skeletal muscle ryanodine receptor channels under near-physiological ionic conditions. J Gen Physiol 122: 407-417.

Kleiber ML, Singh SM. 2009. Divergence of the vertebrate sp1A/ryanodine receptor domain and SOCS box-containing (Spsb) gene family and its expression and regulation within the mouse brain. Genomics 93: 358-366.

Lai FA, Erickson HP, Rousseau E, Liu QY, Meissner G. 1988. Purification and reconstitution of the calcium release channel from skeletal muscle. Nature 331: 315-319.

Lamb GD. 1993. Ca2+ inactivation, Mg2+ inhibition and malignant hyperthermia. J Muscle Res Cell Motil 14: 554-556.

Lanner JT, Georgiou DK, Joshi AD, Hamilton SL. 2010. Ryanodine receptors: structure, expression, molecular details, and function in calcium release. Cold Spring Harb Perspect Biol 2: a003996.

Laver DR. 2007. Ca2+ stores regulate ryanodine receptor Ca2+ release channels via luminal and cytosolic Ca2+ sites. Biophys J 92: 3541-3555.

Laver DR. 2009. Luminal Ca(2+) activation of cardiac ryanodine receptors by luminal and cytoplasmic domains. Eur Biophys J 39: 19-26.

Laver DR, Honen BN. 2008. Luminal Mg2+, a key factor controlling RYR2-mediated Ca2+ release: cytoplasmic and luminal regulation modeled in a tetrameric channel. J Gen Physiol 132: 429-446.

Laver DR, Baynes TM, Dulhunty AF. 1997. Magnesium inhibition of ryanodine-receptor calcium channels: Evidence for two independent mechanisms. J Membr Biol 156: 213-229.

Li P, Chen SR. 2001. Molecular basis of Ca(2)+ activation of the mouse cardiac Ca(2)+ release channel (ryanodine receptor). J Gen Physiol 118: 33-44.

Liu Z, Zhang J, Li P, Chen SR, Wagenknecht T. 2002. Three-dimensional reconstruction of the recombinant type 2 ryanodine receptor and localization of its divergent region 1. J Biol Chem 277: 46712-46719.

Liu Z, Zhang J, Wang R, Wayne Chen SR, Wagenknecht T. 2004. Location of divergent region 2 on the three-dimensional structure of cardiac muscle ryanodine receptor/calcium release channel. J Mol Biol 338: 533-545.

Liu Z, Wang R, Zhang J, Chen SR, Wagenknecht T. 2005. Localization of a disease-associated mutation site in the three-dimensional structure of the cardiac muscle ryanodine receptor. J Biol Chem 280: 37941-37947.

Liu Z, Zhang J, Sharma MR, Li P, Chen SR, Wagenknecht T. 2001. Three-dimensional reconstruction of the recombinant type 3 ryanodine receptor and localization of its amino terminus. Proc Natl Acad Sci U S A 98: 6104-6109.

Lobo PA, Van Petegem F. 2009. Crystal structures of the N-terminal domains of cardiac and skeletal muscle ryanodine receptors: insights into disease mutations. Structure 17: 1505-1514.

Lopez-Lopez JR, Shacklock PS, Balke CW, Wier WG. 1995. Local calcium transients triggered by single L-type calcium channel currents in cardiac cells. Science 268: 1042-1045.

Lukyanenko V, Gyorke I, Subramanian S, Smirnov A, Wiesner TF, Gyorke S. 2000. Inhibition of Ca(2+) sparks by ruthenium red in permeabilized rat ventricular myocytes. Biophys J 79: 1273-1284.

Marjamaa A, Laitinen-Forsblom P, Lahtinen AM, Viitasalo M, Toivonen L, Kontula K, Swan H. 2009. Search for cardiac calcium cycling gene mutations in familial ventricular arrhythmias resembling catecholaminergic polymorphic ventricular tachycardia. BMC Med Genet 10: 12.

Marx SO, Marks AR. 2002. Regulation of the ryanodine receptor in heart failure. Basic Res Cardiol 97 Suppl 1: I49-51.

Marx SO, Reiken S, Hisamatsu Y, Gaburjakova M, Gaburjakova J, Yang YM, Rosemblit N, Marks AR. 2001. Phosphorylation-dependent regulation of ryanodine receptors: a novel role for leucine/isoleucine zippers. J Cell Biol 153: 699-708.

Medeiros-Domingo A, Bhuiyan ZA, Tester DJ, Hofman N, Bikker H, van Tintelen JP, Mannens MM, Wilde AA, Ackerman MJ. 2009. The RYR2-encoded ryanodine receptor/calcium release channel in patients diagnosed previously with either catecholaminergic polymorphic ventricular tachycardia or genotype negative, exercise-induced long QT syndrome: a comprehensive open reading frame mutational analysis. J Am Coll Cardiol 54: 2065-2074.

Meissner G. 1994. Ryanodine receptor/Ca2+ release channels and their regulation by endogenous effectors. Annu Rev Physiol 56: 485-508.

Meissner G. 2002. Regulation of mammalian ryanodine receptors. Front Biosci 7: d2072-2080.

Meissner G. 2004. Molecular regulation of cardiac ryanodine receptor ion channel. Cell Calcium 35: 621-628.

Meissner G, Henderson JS. 1987. Rapid calcium release from cardiac sarcoplasmic reticulum vesicles is dependent on Ca2+ and is modulated by Mg2+, adenine nucleotide, and calmodulin. J Biol Chem 262: 3065-3073.

Mejia-Alvarez R, Kettlun C, Rios E, Stern M, Fill M. 1999. Unitary Ca2+ current through cardiac ryanodine receptor channels under quasi-physiological ionic conditions. J Gen Physiol 113: 177-186.

Milting H, Lukas N, Klauke B, Korfer R, Perrot A, Osterziel KJ, Vogt J, Peters S, Thieleczek R, Varsanyi M. 2006. Composite polymorphisms in the ryanodine receptor 2 gene associated with arrhythmogenic right ventricular cardiomyopathy. Cardiovasc Res 71: 496-505.

Murzin AG, Lesk AM, Chothia C. 1992. beta-Trefoil fold. Patterns of structure and sequence in the Kunitz inhibitors interleukins-1 beta and 1 alpha and fibroblast growth factors. J Mol Biol 223: 531-543.

Ono M, et al. 2010. Dissociation of calmodulin from cardiac ryanodine receptor causes aberrant Ca(2+) release in heart failure. Cardiovasc Res 87: 609-617.

Orlova EV, Serysheva II, van Heel M, Hamilton SL, Chiu W. 1996. Two structural configurations of the skeletal muscle calcium release channel. Nat Struct Biol 3: 547-552.

Parker I, Zang WJ, Wier WG. 1996. Ca2+ sparks involving multiple Ca2+ release sites along Z-lines in rat heart cells. J Physiol (Lond) 497: 31-38.

Perez CF, Mukherjee S, Allen PD. 2003. Amino acids 1-1,680 of ryanodine receptor type 1 hold critical determinants of skeletal type for excitation-contraction coupling. Role of divergence domain D2. J Biol Chem 278: 39644-39652.

Ponting C, Schultz J, Bork P. 1997. SPRY domains in ryanodine receptors (Ca(2+)-release channels). Trends Biochem Sci 22: 193-194.

Ponting CP. 2000. Novel repeats in ryanodine and IP3 receptors and protein O-mannosyltransferases. Trends Biochem Sci 25: 48-50.

Protasi F. 2002. Structural interaction between RYRs and DHPRs in calcium release units of cardiac and skeletal muscle cells. Front Biosci 7: d650-658.

Qin J, Valle G, Nani A, Nori A, Rizzi N, Priori SG, Volpe P, Fill M. 2008. Luminal Ca2+ regulation of single cardiac ryanodine receptors: insights provided by calsequestrin and its mutants. J Gen Physiol 131: 325-334.

Rhodes DA, de Bono B, Trowsdale J. 2005. Relationship between SPRY and B30.2 protein domains. Evolution of a component of immune defence? Immunology 116: 411-417.

Rios E, Brum G. 1987. Involvement of dihydropyridine receptors in excitation-contraction coupling in skeletal muscle. Nature 325: 717-720.

Rios E, Karhanek M, Ma J, Gonzalez A. 1993. An allosteric model of the molecular interactions of excitation-contraction coupling in skeletal muscle. J Gen Physiol 102: 449-481.

Sali A, Blundell TL. 1993. Comparative protein modelling by satisfaction of spatial restraints. J Mol Biol 234: 779-815.

Samso M, Wagenknecht T. 2002. Apocalmodulin and Ca2+-calmodulin bind to neighboring locations on the ryanodine receptor. J Biol Chem 277: 1349-1353.

Samso M, Feng W, Pessah IN, Allen PD. 2009. Coordinated movement of cytoplasmic and transmembrane domains of RyR1 upon gating. PLoS Biol 7: e85.

Santana LF, Cheng H, Gomez AM, Cannell MB, Lederer WJ. 1996. Relation between the sarcolemmal Ca2+ current and Ca2+ sparks and local control theories for cardiac excitation-contraction coupling. Circ Res 78: 166-171.

Schiefer A, Meissner G, Isenberg G. 1995. Ca2+ activation and Ca2+ inactivation of canine reconstituted cardiac sarcoplasmic reticulum Ca(2+)-release channels. J Physiol (Lond) 489: 337-348.

Serysheva, II, Hamilton SL, Chiu W, Ludtke SJ. 2005. Structure of Ca2+ release channel at 14 A resolution. J Mol Biol 345: 427-431.

Serysheva, II, Schatz M, van Heel M, Chiu W, Hamilton SL. 1999. Structure of the skeletal muscle calcium release channel activated with Ca2+ and AMP-PCP. Biophys J 77: 1936-1944.

Serysheva, II, Ludtke SJ, Baker ML, Cong Y, Topf M, Eramian D, Sali A, Hamilton SL, Chiu W. 2008. Subnanometer-resolution electron cryomicroscopy-based domain models for the cytoplasmic region of skeletal muscle RyR channel. Proc Natl Acad Sci U S A 105: 9610-9615.

Shannon TR, Guo T, Bers DM. 2003. Ca2+ scraps: local depletions of free [Ca2+] in cardiac sarcoplasmic reticulum during contractions leave substantial Ca2+ reserve. Circ Res 93: 40-45.

Sharma MR, Jeyakumar LH, Fleischer S, Wagenknecht T. 2000. Three-dimensional structure of ryanodine receptor isoform three in two conformational states as visualized by cryo-electron microscopy. J Biol Chem 275: 9485-9491.

Sharma MR, Penczek P, Grassucci R, Xin HB, Fleischer S, Wagenknecht T. 1998. Cryoelectron microscopy and image analysis of the cardiac ryanodine receptor. J Biol Chem 273: 18429-18434.

Shatsky M, Nussinov R, Wolfson HJ. 2004. A method for simultaneous alignment of multiple protein structures. Proteins 56: 143-156.

Smith JS, Imagawa T, Ma J, Fill M, Campbell KP, Coronado R. 1988. Purified ryanodine receptor from rabbit skeletal muscle is the calcium-release channel of sarcoplasmic reticulum. J Gen Physiol 92: 1-26.

Sorrentino V. 1995. The ryanodine receptor family of intracellular calcium release channels. Adv Pharmacol 33: 67-90.

Stern MD. 1992. Theory of excitation - contraction coupling in cardiac muscle. Biophys J 63: 497-517.

Strahl-Bolsinger S, Scheinost A. 1999. Transmembrane topology of pmt1p, a member of an evolutionarily conserved family of protein O-mannosyltransferases. J Biol Chem 274: 9068-9075.

Takasago T, Imagawa T, Furukawa K, Ogurusu T, Shigekawa M. 1991. Regulation of the cardiac ryanodine receptor by protein kinase-dependent phosphorylation. J Biochem 109: 163-170.

Tateishi H, Yano M, Mochizuki M, Suetomi T, Ono M, Xu X, Uchinoumi H, Okuda S, Oda T, Kobayashi S, Yamamoto T, Ikeda Y, Ohkusa T, Ikemoto N, Matsuzaki M. 2009. Defective domain-domain interactions within the ryanodine receptor as a critical cause of diastolic Ca2+ leak in failing hearts. Cardiovasc Res 81: 536-545.

Terentyev D, Kubalova Z, Valle G, Nori A, Vedamoorthyrao S, Terentyeva R, Viatchenko-Karpinski S, Bers DM, Williams SC, Volpe P, Gyorke S. 2008. Modulation of SR Ca release by luminal Ca and calsequestrin in cardiac myocytes: effects of CASQ2 mutations linked to sudden cardiac death. Biophys J 95: 2037-2048.

Tester DJ, Kopplin LJ, Will ML, Ackerman MJ. 2005. Spectrum and prevalence of cardiac ryanodine receptor (RyR2) mutations in a cohort of unrelated patients referred explicitly for long QT syndrome genetic testing. Heart Rhythm 2: 1099-1105.

Tester DJ, Arya P, Will M, Haglund CM, Farley AL, Makielski JC, Ackerman MJ. 2006. Genotypic heterogeneity and phenotypic mimicry among unrelated patients referred for catecholaminergic polymorphic ventricular tachycardia genetic testing. Heart Rhythm 3: 800-805.

Tung CC, Lobo PA, Kimlicka L, Van Petegem F. 2010. The amino-terminal disease hotspot of ryanodine receptors forms a cytoplasmic vestibule. Nature 468: 585-588.

Unnerstale S, Lind J, Papadopoulos E, Maler L. 2009. Solution structure of the HsapBK K+ channel voltage-sensor paddle sequence. Biochemistry 48: 5813-5821.

Valdivia HH, Kaplan JH, Ellis-Davies GC, Lederer WJ. 1995. Rapid adaptation of cardiac ryanodine receptors: modulation by Mg2+ and phosphorylation. Science 267: 1997-2000.

Velez P, Gyorke S, Escobar AL, Vergara J, Fill M. 1997. Adaptation of single cardiac ryanodine receptor channels. Biophys J 72: 691-697.

Wagenknecht T, Samso M. 2002. Three-dimensional reconstruction of ryanodine receptors. Front Biosci 7: d1464-1474.

Wang R, Zhong X, Meng X, Koop A, Tian X, Jones PP, Fruen BR, Wagenknecht T, Liu Z, Chen SR. 2011. Localization of the dantrolene-binding sequence near the FK506-binding protein-binding site in the three-dimensional structure of the ryanodine receptor. J Biol Chem 286: 12202-12212.

Wang SQ, Song LS, Lakatta EG, Cheng H. 2001. Ca2+ signalling between single L-type Ca2+ channels and ryanodine receptors in heart cells. Nature 410: 592-596.

Wang SQ, Stern MD, Rios E, Cheng H. 2004. The quantal nature of Ca2+ sparks and in situ operation of the ryanodine receptor array in cardiac cells. Proc Natl Acad Sci U S A 101: 3979-3984.

Whitmore L, Wallace BA. 2004. DICHROWEB, an online server for protein secondary structure analyses from circular dichroism spectroscopic data. Nucleic Acids Res 32: W668-673.

Williams AJ. 1992. Ion conduction and discrimination in the sarcoplasmic reticulum ryanodine receptor/calcium-release channel. J Muscle Res Cell Motil 13: 7-26.

Williams AJ, West DJ, Sitsapesan R. 2001. Light at the end of the Ca(2+)-release channel tunnel: structures and mechanisms involved in ion translocation in ryanodine receptor channels. Q Rev Biophys 34: 61-104.

Witcher DR, Kovacs RJ, Schulman H, Cefali DC, Jones LR. 1991. Unique phosphorylation site on the cardiac ryanodine receptor regulates calcium channel activity. J Biol Chem 266: 11144-11152.

Woo JS, Imm JH, Min CK, Kim KJ, Cha SS, Oh BH. 2006. Structural and functional insights into the B30.2/SPRY domain. EMBO J 25: 1353-1363.

Xiong L, Zhang JZ, He R, Hamilton SL. 2006. A Ca2+-binding domain in RyR1 that interacts with the calmodulin binding site and modulates channel activity. Biophys J 90: 173-182.

Xu L, Meissner G. 1998. Regulation of cardiac muscle Ca2+ release channel by sarcoplasmic reticulum lumenal Ca2+. Biophys J 75: 2302-2312.

Xu L, Mann G, Meissner G. 1996. Regulation of cardiac Ca2+ release channel (ryanodine receptor) by Ca2+, H+, Mg2+, and adenine nucleotides under normal and simulated ischemic conditions. Circ Res 79: 1100-1109.

Xu X, Bhat MB, Nishi M, Takeshima H, Ma J. 2000. Molecular cloning of cDNA encoding a drosophila ryanodine receptor and functional studies of the carboxyl-terminal calcium release channel. Biophys J 78: 1270-1281.

Xu X, et al. 2010. Defective calmodulin binding to the cardiac ryanodine receptor plays a key role in CPVT-associated channel dysfunction. Biochem Biophys Res Commun 394: 660-666.

Yamamoto T, Ikemoto N. 2002. Peptide probe study of the critical regulatory domain of the cardiac ryanodine receptor. Biochem Biophys Res Commun 291: 1102-1108.

Yamamoto T, El-Hayek R, Ikemoto N. 2000. Postulated role of interdomain interaction within the ryanodine receptor in Ca(2+) channel regulation. J Biol Chem 275: 11618-11625.

Yamamoto T, Yano M, Xu X, Uchinoumi H, Tateishi H, Mochizuki M, Oda T, Kobayashi S, Ikemoto N, Matsuzaki M. 2008. Identification of target domains of the cardiac ryanodine receptor to correct channel disorder in failing hearts. Circulation 117: 762-772.

Yang Z, Ikemoto N, Lamb GD, Steele DS. 2006. The RyR2 central domain peptide DPc10 lowers the threshold for spontaneous Ca2+ release in permeabilized cardiomyocytes. Cardiovasc Res 70: 475-485.

Yano M, Yamamoto T, Ikeda Y, Matsuzaki M. 2006. Mechanisms of Disease: ryanodine receptor defects in heart failure and fatal arrhythmia. Nat Clin Pract Cardiovasc Med 3: 43-52.

Yao S, Liu MS, Masters SL, Zhang JG, Babon JJ, Nicola NA, Nicholson SE, Norton RS. 2006. Dynamics of the SPRY domain-containing SOCS box protein 2: flexibility of key functional loops. Protein Sci 15: 2761-2772.

Yuchi Z, Van Petegem F. 2011. Common allosteric mechanisms between ryanodine and inositol-1,4,5-trisphosphate receptors. Channels (Austin) 5: 120-123.

Zahradnik I, Gyorke S, Zahradnikova A. 2005. Calcium activation of ryanodine receptor channels--reconciling RyR gating models with tetrameric channel structure. J Gen Physiol 126: 515-527.

Zahradnikova A, Zahradnik I. 1999. Analysis of calcium-induced calcium release in cardiac sarcoplasmic reticulum vesicles using models derived from single-channel data. Biochim Biophys Acta 1418: 268-284.

Zahradnikova A, Valent I, Zahradnik I. 2010. Frequency and release flux of calcium sparks in rat cardiac myocytes: a relation to RYR gating. J Gen Physiol 136: 101-116.

Zahradnikova A, Zahradnik I, Gyorke I, Gyorke S. 1999. Rapid activation of the cardiac ryanodine receptor by submillisecond calcium stimuli. J Gen Physiol 114: 787-798.

Zahradnikova A, Dura M, Gyorke I, Escobar AL, Zahradnik I, Gyorke S. 2003. Regulation of dynamic behavior of cardiac ryanodine receptor by Mg2+ under simulated physiological conditions. Am J Physiol Cell Physiol 285: C1059-1070.

Zhang J, Liu Z, Masumiya H, Wang R, Jiang D, Li F, Wagenknecht T, Chen SR. 2003. Three-dimensional localization of divergent region 3 of the ryanodine receptor to the clamp-shaped structures adjacent to the FKBP binding sites. J Biol Chem 278: 14211-14218.

Zhao M, Li P, Li X, Zhang L, Winkfein RJ, Chen SR. 1999. Molecular identification of the ryanodine receptor pore-forming segment. J Biol Chem 274: 25971-25974.

Zimanyi I, Pessah IN. 1991. Comparison of [3H]ryanodine receptors and Ca++ release from rat cardiac and rabbit skeletal muscle sarcoplasmic reticulum. J Pharmacol Exp Ther 256: 938-946.